International Journal of Concrete Structures and Materials

RESEARCH

Open Access

Hydration Characteristics of Slag-$Ca(OH)_2$-Al_2O_3 Binder in a 60 °C Curing Environment with Brine as Mixing Water

Choonghyun Kang[1], Taewan Kim[2*], Yong-Myung Park[2*] and Ki-Young Seo[3]

Abstract

Recently, research results on PC-based or alkali-activated slag cement (AASC) using seawater as mixing water have been reported. Unlike seawater, reverse osmosis brine (brine) is waste discharged into the ocean from seawater desalination plants. There is a need to develop new and effective methods of disposing or utilizing brine to reduce marine pollution, protect marine ecosystems, and increase marine plant construction. However, research on cement or concrete using brine as a mixing water is very limited. Brine has almost the same composition as seawater, and the ion concentration is 2–4 times higher. Therefore, it is believed that new methods of using brine can be investigated and developed based on existing research and experimental results on seawater. The effects of brine and aluminum oxide (AO) on activated slag with calcium hydroxide (CH) were investigated for hydration and mechanical properties. 5% and 10% of CH were used, and samples using fresh water (FC) were prepared at the same time for comparison with brine. The slag sample without CH has a low initial (1 and 3d) strength of about 10 MPa for both FC and brine, but increases rapidly from 7d. Incorporation of CH was effective in improving the mechanical performance of FC and brine samples. In addition, the brine sample exhibited higher strength than the FC sample because it formed fewer C3AH6 phases that cause volume instability than the FC sample and affected the hydration promotion of slag particles. And more calcite phases were observed in the brine samples than in the FC samples. Through this study, the possibility of using brine as a building material was confirmed. In addition, the effect of chloride ion adsorption of slag mixed with AO and CH on the physical properties and mechanical performance of the hydration reaction was confirmed.

Keywords Reverse osmosis brine, Slag, Aluminum oxide, Calcium hydroxide, Hydration, Construction material

1 Introduction

There is severe shortage of drinking water due to climate change and freshwater pollution. Thus, securing sufficient quality drinking water for a growing population is becoming an important issue. Recently, the construction of desalination plants, which is one of the methods for solving this shortage, is increasing (Jones et al., 2019; Panagopoulos et al., 2019). There are various desalination methods, but reverse osmosis is the most widely used (Portillo et al., 2014; Qasim et al., 2019). Most of the reverse osmosis brine (brine), generated after desalination in a seawater desalination plant is discarded into the ocean. The composition of brine is same as that of

Journal information: ISSN 1976-0485 / eISSN 2234-1315.

*Correspondence:
Taewan Kim
taewan-kim@pusan.ac.kr; ring2014@naver.com
Yong-Myung Park
ympk@pusan.ac.kr
[1] Department of Ocean Civil Engineering, Gyeongsang National University, Tongyeong 53064, Republic of Korea
[2] Department of Civil Engineering, Pusan National University, Busan 46241, Republic of Korea
[3] HK E&C, 31, Beomeocheon-ro, Geumjeong-gu, Busan 46220, Republic of Korea

seawater, but it is higher in concentration. Chloride ions are about 2–5 times higher in brine than in seawater. The brine also includes some other chemicals that are used during certain processes in desalination plants. The release of brine into the ocean destroys the nearby marine ecosystem (Koch et al., 2007; Torchette, 2007). Therefore, it is necessary to develop a new application method for brine. In this study, we intend to examine the use of brine for construction materials experimentally.

Blast furnace slag is a pozzolanic material that has been used in cement/concrete for a long time (Ortega et al., 2012; Shumuye et al., 2019; Yang et al., 2020a). So far, among the various advantages of blast furnace slag, there are reports on its ability to immobilize chloride ions. Studies have been reported on blast furnace slag cement exposed to an environment with chloride ions or mixed with a chloride or seawater solution (Jin et al., 2022; Li et al., 2020, 2021; Jin et al., 2021; Liu et al., 2021). Recently, research results on the effect of seawater on alkali-activated cement or geopolymer were also published (Jun et al., 2020; Kang & Kim, 2020). These studies revealed that seawater or chloride solutions promote hydration in the early-age stage of binders containing slag (Kang & Kim 2020l; Jun et al., 2020; Liu et al., 2021). Consequently, it was observed to form a high strength and dense pore structure (Liu et al., 2021). This pore structure improvement improves the mechanical performance of slag-based high-volume slag cement and alkali-activated slag cement (AASC).

Studies on the adsorption of chloride ions are divided into two types: physical adsorption and chemical adsorption (Hussain & Al-Saadoum 1990; Chang, 2017). Chemical absorption consists of the formation of hydration reactants such as Friedel's salts. Physical adsorption is known to be mainly achieved using calcium silicate hydrate (CSH) gel (Zheng et al., 2021). Aluminum is gaining attention as an important factor for the adsorption of such chloride ions. It has been reported that aluminum ions play a major role in forming Friedel's salt, an important binder in chemical adsorption (Saillio et al., 2014; Yuan et al., 2009). So, cement/concrete exposed to seawater or chloride environment is mixed with an aluminum-rich material such as are metakaolin, fly ash, and nano-Al_2O_3 particles (Chen et al., 2020; Gbozee et al., 2018; Liu et al., 2019; Wang et al., 2019a, 2019b; Yang et al., 2019). Materials containing such aluminum components improve the adsorption effect of chloride ions by forming Friedel's salt through the hydration reaction of cement/concrete. Other factors such as pH, carbonation, admixture materials, curing temperature, and exposure environment also affect the adsorption effect of chloride ions (Chang, 2017; Chang et al., 2019; Galan & Glasser, 2015; Wang et al., 2020; Zheng et al., 2021). However, considering hydration reactants, the supply of aluminum is the most crucial factor that could confirm the adsorption effect of chloride ions. In another study, calcium ion was reported as an important factor in adsorption of chloride ion (De Weerdt et al., 2015; Pruckner & Gjørv, 2004; Zhu et al., 2012).

Cement using seawater or mixed water containing chloride ions has limitations as it cannot be used with steel. As a result, the scope of application is very limited to the manufacture of bricks, blocks, panels, small structural members or concrete using fiber or FRP without steel. Also, unlike seawater, research on cement or concrete using brine is more limited compared to seawater. However, unlike seawater, brine is discharged from a seawater desalination plant and has gone through a certain sedimentation and filtration process, so there are no organic substances, impurities, or harmful substances. This can dramatically reduce the cost and time required for the pretreatment process required to use seawater as mixing water. Therefore, compared to seawater that requires pretreatment, brine can be used as blended water immediately after being discharged from the seawater desalination plant. If brine is applied to construction materials as a new use, it is expected to contribute to environmentally friendly concrete manufacturing as well as preserving the marine environment. To do so, it is necessary to find the optimal mixing and process for manufacturing concrete products using brine as a mixing water. And research and attempts on eco-friendly cement made of this combination of brine and AASC are rare compared to those using seawater.

This study considered the following three points to apply to eco-friendly cement using 100% slag as a binder. (i) A high temperature curing method of 60 °C was applied to promote the hydration reaction of slag and improve the problem of initial strength reduction. (ii) Calcium hydroxide ($Ca(OH)_2$; CH) was substituted at 5% and 10% to increase the effect of promoting hydration of slag and immobilizing chloride ions. (iii) To increase the effect of immobilizing chloride ions, 5% of aluminum oxide (Al_2O_3; AO) was substituted. For comparison with brine, samples using fresh water (FC) as the mixing water were also prepared for the same AO and CH concentrations. The three considered research and experiment requirements are expected to contribute to the basic data or expanded application required for the manufacture of eco-friendly cement/concrete products using brine and slag as binders in the future. It is believed that this can be used to develop a process that can quickly and in large quantities manufacture products of sufficient quality as construction members by applying various admixtures and by-products containing calcium and aluminum and curing at high temperatures.

Table 1 Chemical components properties in slag

	Chemical components (%)						
	SiO_2	Al_2O	Fe_2O	MgO	CaO	K_2O	SO_3
Slag	33.86	9.37	0.74	4.82	46.50	0.31	3.58

Table 2 Reverse osmosis brine composition (ppm)

	Na^+	Ca^{2+}	K^+	Mg^{2+}	SO_4^{2-}	Cl^-
Brine	1,618.2	575.4	597.1	1,830.9	3,784.5	27,236.1
Fresh water	5.1	19.3	2.4	3.5	N.D	N.D

(N.D: Not Detected)

2 Materials and Experiments

2.1 Materials

Table 1 shows the chemical composition of the ground granulated blast furnace slag (slag) used in the experiment. The slag used in the experiment was supplied by a steel mill by-product processing company (KRT Co.) located in Pohang, Korea. The slag has a density of 2.89 g/cm^3, 4200 cm^2/kg fineness, and 0.96% LOI. The brine was used as mix water, and fresh water (FC) was also mixed for comparison. Brine was analyzed for composition by inductively coupled plasma optical emission spectroscopy and ion chromatography. Table 2 shows the results of the brine analysis. Aluminum oxide (Al_2O_3) is a white powder reagent with a purity of 99.0% from SAMCHUN chemical (KOREA).

2.2 Experiments

The concentration of AO was determined to be 5% by referring to the mechanical performance and the adsorption capacity of chloride ions from the reports of various previous research results using AO or nano-Al_2O_3. Most nano-Al_2O_3 has a low substitution rate of 4.0% or less based on the weight of the binder (Chen et al., 2020; Liu et al., 2019; Yang et al., 2019, 2020b). This is because a large specific surface area according to the extremely small particle size of nano-Al2O3 requires a large number of mixed-water, which affects the decrease in fluidity. In the case of supplementary cementitious materials (SCM) used as sources of AO ions, such as metakaoline, they show high AO concentrations of more than 5%, but it is difficult to clearly know the concentrations eluted from SCM (Li et al., 2023; Nazari & Riahi, 2011). However, studies using 5% or more of AO powder have been reported in some previous studies. As the concentration of AO increased, the chloride ion adsorption capacity increased and the mechanical performance also improved (Wang et al., 2019b). In addition, there was a study on the adsorption and movement of chloride ions using AO/nano-Al_2O_3 in parallel with CaO or $Ca(OH)_2$ (Fan et al., 2023; Yang et al., 2022). Based on the results of these previous studies, in this study, the concentrations of $Ca(OH)_2$ were selected as 5 and 10% (Yang et al., 2022).

Table 3 Experimental samples and their mix ratios (wt.%)

	Slag	Al_2O_3	$Ca(OH)_2$	Mix water
FC0	95	5	0	Fresh water
FC5	90	5	5	Fresh water
FC10	85	5	10	Fresh water
BC0	95	5	0	Brine
BC5	90	5	5	Brine
BC10	85	5	10	Brine

Therefore, the early–age mechanical properties were improved in this experiment by setting the curing temperature to 60 °C at 5% AO concentration. Table 3 shows the composition ratio of the six samples evaluated and the binder. "F" indicates the sample containing fresh water as the mixed water, and "B" indicates the sample containing brine. "C0" stands for without CH, and "C5" and "C10" refer to a mixture of 5% and 10% CH, respectively. All samples were prepared with the same 0.40 water-binder ratio.

The samples were mixed according to the mixing method suggested in ASTM C305 (ASTM, 2020). The mixed paste was placed in a 25 × 25 × 25 mm cubic mold, vibrated for 10 s, and stored in a chamber with a temperature of 23 ± 2 °C and relative humidity (RH) of 90 ± 5%. After one day, the mold was removed, and the sample was stored in a chamber with the same temperature and humidity (23 ± 2 °C, RH 90 ± 5%).

The specimen's compressive strength was measured at 1, 3, 7, and 28 d, and the samples' average value was

calculated. The hydration reaction was observed by X-ray diffraction (XRD; Malvern Panalytical, X'pert 3) and thermal analysis by thermogravimetric (TG; TA Instruments, TGA 55), differential thermal analysis (DTA; TG; TA Instruments, TGA 55), and scanning electron microscopy (SEM; Zeiss, SUPRA 40VP). For XRD, the compressive strengths of the 1, 3, 7, and 28 d samples were measured. The crushed pieces were hydrated with an isopropyl solution, and then vacuum dried to form a powder. Measurement conditions for XRD analysis were Cu-K radiation with λ = 1.54443 Å, 40 kV voltage, 0.017° (2θ) step size, 5–60° range. Thermal analyses were performed on the 1 and 28 d samples. The temperature ranged from 30 to 800 °C, increasing at a rate of 10 °C/min. Measurements were performed on N_2 gas. SEM images of the 28 d samples were obtained with a 15 keV acceleration voltage. Before measurement, the samples were immersed in isopropyl alcohol for 24 h, dried in a vacuum desiccator for 48 h, and coated with platinum. Fourier transform infrared spectroscopy (FT-IR; Thermo Fisher, Nicolet iS50) was performed to confirm the effect of brine and CH on the hydration products of the slag. FT-IR was measured in the spectral wavenumber range of 400–4000 cm^{-1} using an IS50 instrument from ThermoFisher Scientific Nicolet. Water absorption was measured according to ASTM C1403 (ASTM, 2022) for the 28 d samples. The dry density was calculated using Eq. (1).

$$\rho_d = \frac{m_d}{V} \tag{1}$$

where ρ_d is the dry density, m_d is the sample's mass after oven drying at 105 ± 5 °C for 24 h, and V is the volume of the sample.

3 Results and Discussion

3.1 Compressive Strength

Fig. 1 shows the results of measuring the compressive strength values depending on the type of mixing water and the concentration of CH. The compressive strength measurement results of specimens using fresh water as the mixing water are shown in Fig. 1a. As the concentration of CH increased from 0 to 10%, the compressive strength values increased on all strength measurement days. Therefore, the 10% CH test specimen showed the highest strength value. The 0% CH specimen showed similar compressive strength values at 1d and 3d and showed a very slight increase, but increased rapidly at 7d. On the other hand, the 5% and 10% CH specimens showed high strength values of 20 MPa or more from 1d and gradually increased compressive strength values over time. Therefore, it is judged that the mixing of CH contributes to the improvement of mechanical performance by accelerating the initial hydration reaction of the slag.

The strength measurement results of the specimens using brine as the mixing water are shown in Fig. 1b. Similar to the FC samples in Fig. 1a, the strength also improved as the concentration of CH increased. In addition, the 0% CH test specimen showed a slight increase in strength until 3d, but showed a rapid increase at 7d, which is a similar tendency to the 0% CH specimen of FC.

At 7d and 28d for both FC and brine specimens, the difference in compressive strength values between 5 and 10% CH specimens was small. This is a decrease in the strength change rate compared to the difference in strength values at 1d and 3d. That is, it can be inferred that CH has a great effect on the hydration response and

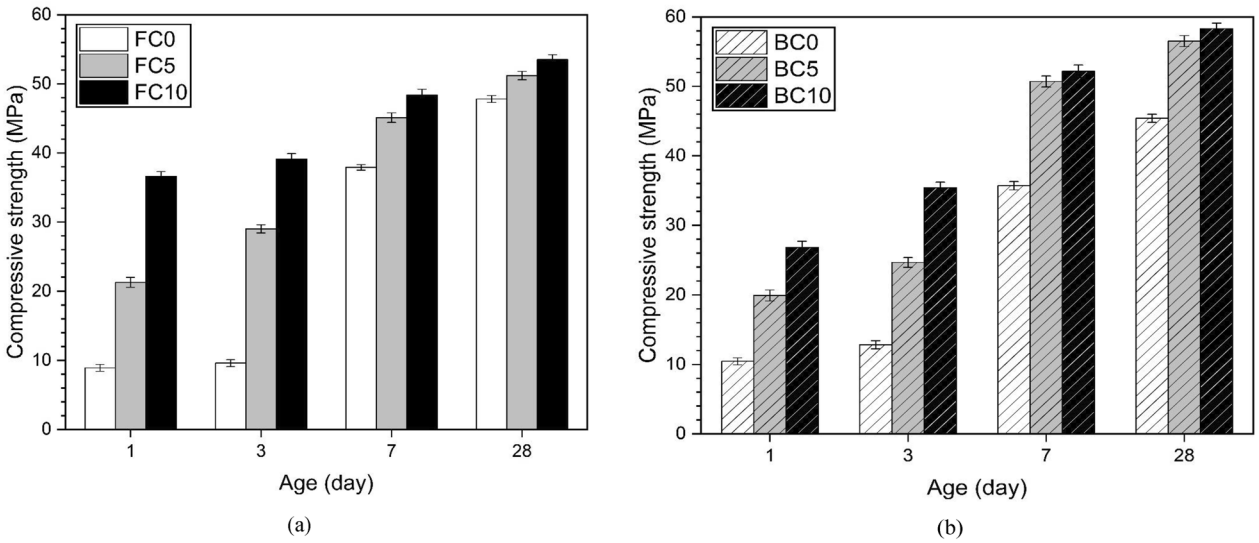

Fig. 1 Compressive strengths by type of mix water, (**a**) fresh water, (**b**) brine

mechanical performance in the early-age stages (1d and 3d) in both FC and brine specimens.

The results of comparing the compressive strength values of the FC and brine specimens at each measurement age are shown in Fig. 2. Fig. 2a, b show the strength values of the FC and brine test specimens at 1d and 3d. In the 0% CH test specimen, the brine showed a slightly higher strength than the FC. However, 5 and 10% CH showed higher values of FC specimens. The strength values at 7d and 28d show opposite trends to those at early-age. In Fig. 2c, d, the 0% CH specimens show a higher value in FC than the brine specimens. Also, 5 and 10% CH specimens showed higher compressive strength values for brine than for FC.

In the 0% CH test specimen, brine contributes to the improvement of the mechanical performance of the slag at early–age 1d and 3d, but the effect decreases after 7d. However, the FC specimens show higher mechanical performance than the brine specimens after 7d. 5 and 10% CH showed more effective mechanical performance of FC specimens at early–age (1d and 3d), but brine showed a higher strength improvement effect at late–age (7d and 28d).

Therefore, in the results of mixtures mixed with CH, brine has a limited effect on improving the mechanical performance of slag in the early-age stage within 3d, but the improvement effect is clearly shown over time after 7d.

Previous studies using seawater reported that it promoted the hydration of slag and the effect of improving the early-age strength (Jun et al., 2021; Ren et al., 2021; Wang et al., 2020; Zhang et al., 2021). However, the early–age strength enhancement effect of brine was not

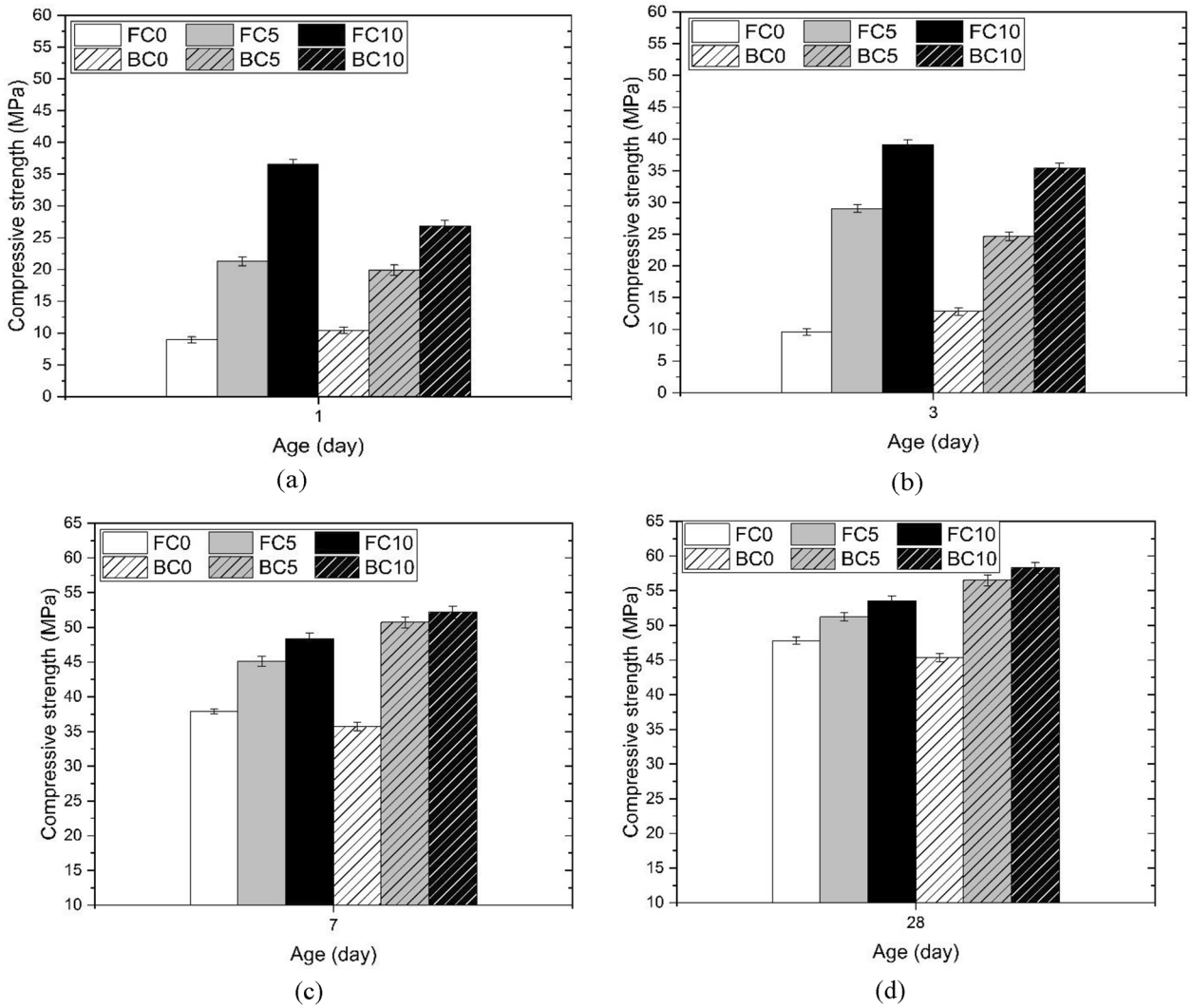

Fig. 2 Strengths of fresh water and brine samples by age, (**a**) 1 d, (**b**) 3 d, (**c**) 7 d, and (**d**) 28 d

shown in the slag–Al_2O_3–$Ca(OH)_2$ mixed binder under high temperature curing conditions of 60 °C.

Table 4 summarizes the calculated strength change rates for the 5 and 10% CH specimens based on the compressive strength value of the 0% CH specimen. In Table 4, specimens substituted with 5 and 10% CH using fresh water as the mixing water show a high increase in compressive strength of 200–400% for 1d and 3d. However, brine specimens showed a relatively low strength improvement in the range of 190–280%. The strength increase rate at 7d and 28d was higher in brine specimens than in fresh water (FC specimens). In other words, the strength increase rate in early-age up to 3d was higher for FC specimens, but it was higher in brine specimens from 7d to late-age. This is believed to be because various ions contained in brine affect the formation and phase change of hydration reactants.

3.2 Hydration Products

Fig. 3 shows each sample's XRD analysis results of the hydration reactants at 1, 7, and 28d. Commonly observed hydration reactants in FC and brine are CSH(I), CSH, calcite, C3AH6, C2ASH8, C4AH13, monocarboaluminate, and hydrotalcite. Friedel's salt was also observed in the brine specimens.

In Fig. 3, the brine specimens (BC) show a relatively lower C2ASH8 peak intensity than the fresh water specimens (FC). This difference can be explained in two ways. For one, the conversion of C2ASH8 to Friedel's salt could explain the weak peak intensity (Ke et al., 2017). In fact, high peak intensity of Fridel's salt was detected in the BC specimens. Another cause may be the conversion of C2ASH8 to C4AH13 (Morsy, 2005). This is confirmed by observing that the C4AH14 peak intensity of the BC specimens is higher than that of the FC. C3AH6 and monocarboaluminate peaks detected in FC were not detected in BC. As expected, it was observed that the intensity of the portlandite peak increased as the concentration of CH increased in the FC and BC specimens. CSH gel showed that the peak intensity increased as the concentration of CH increased. Through this change in peak intensity, it was determined that the increase in the concentration of CH has the effect of promoting the formation of hydration products of slag. It was confirmed that BC and CH cause changes in the hydration reactants of the slag compared to FC.

Table 4 Rate of change in strength at each age for 0% CH

Age (day)	Rate of change in strength (%)			
	FC5	FC10	BC5	BC10
1	238.8	410.8	190.6	256.5
3	302.1	407.3	192.0	275.9
7	119.0	127.7	142.1	146.2
28	107.1	112.0	124.5	128.4

Fig. 4 is an enlarged view of a portion of the XRD graph shown in Fig. 3. The Fig. 4a–c shows peaks of hydration reactants detected in the range of 9–12°. In BC, Friedel's slat peak around 11.2° appears clearly, and 5 and 10% CH show stronger peak intensity than 0% CH. In FC, the peak of hydrotalcite around 11.6° was observed. However, peaks on hydrotalcite were not detected in the BC specimens.

Fig. 4d–f show the peak intensities of portlandite and C3AH6 phases in the 16–19° range. As expected, no portlandite peak was detected at 0% CH, and as the concentration of CH increased, the intensity of the portlandite peak around 8.1° in FC and BC increased. In the case of the FC specimens, a C3AH6 phase peak was observed around 17.3°, and the intensity of the peak increased as the concentration of CH increased. However, the C3AH6 peak of the BC specimens was very weak.

In Fig. 3, the C4AH13 peak intensity of the BC specimens was greater than that of the FC. The C2ASH8 peak intensity of the BC specimens in Fig. 3 was low, suggesting the possibility that it could be a conversion from C2ASH8 to C4AH13 (Morsy, 2005). One of the reasons for the low intensity of the C4AH13 peak in the FC specimens is that the metastable phase C4AH13 is converted to the stable phase C3AH6 (Son et al., 2018; Duran et al., 2016; Ukrinczyk et al., 2007; Janotka, 2001). As a result, the peak intensity of the C4AH13 phase is stronger and the C3AH6 peak is detected with a weak intensity compared to the FC specimen in BC. Looking at these phase detection results, brine interferes with the conversion of C4AH13 to C3AH6, and as a result, the intensity of the C4AH13 peak was strong and the peak intensity of C3AH6 was weak in the BC specimens.

Fig. 4g–i shows the 28–30.5° range for comparison of CSH gel. The peak intensity in the range of 28–30.5° increased with the curing time. This means that the generation of hydration reactants increased due to the hydration reaction of the slag over time. Through comparison of BC and FC specimens, the difference in intensity of CSH gel peaks is small or similar.

The reaction process of the hydration reactant can be expressed as follows. Equations (2) and (3) are C_3AH_6 (Jambunathan et al., 2013; Janotka, 2001), Eq. (4) is C_2ASH_8 (Kang & Kim, 2023), Eq. (5) is calcite (Palin et al., 2016), Eqs. (6) and (7) are monocarboaluminate ($C_4A\underline{C}H_{11}$) (Chang et al., 2022), and Eqs. (8) and (9) are CSH ($C_3S_2H_3$) (Janotka, 2001), Eq. (10) represents hydrotalcite ($M_6A\underline{C}H_4$) (Suescum-Morales et al., 2021), and Eqs. (11) and (12) represent Friedel's salt ($C_4ACl_2H_{10}$) (Shi et al., 2015) (cement chemist notation:

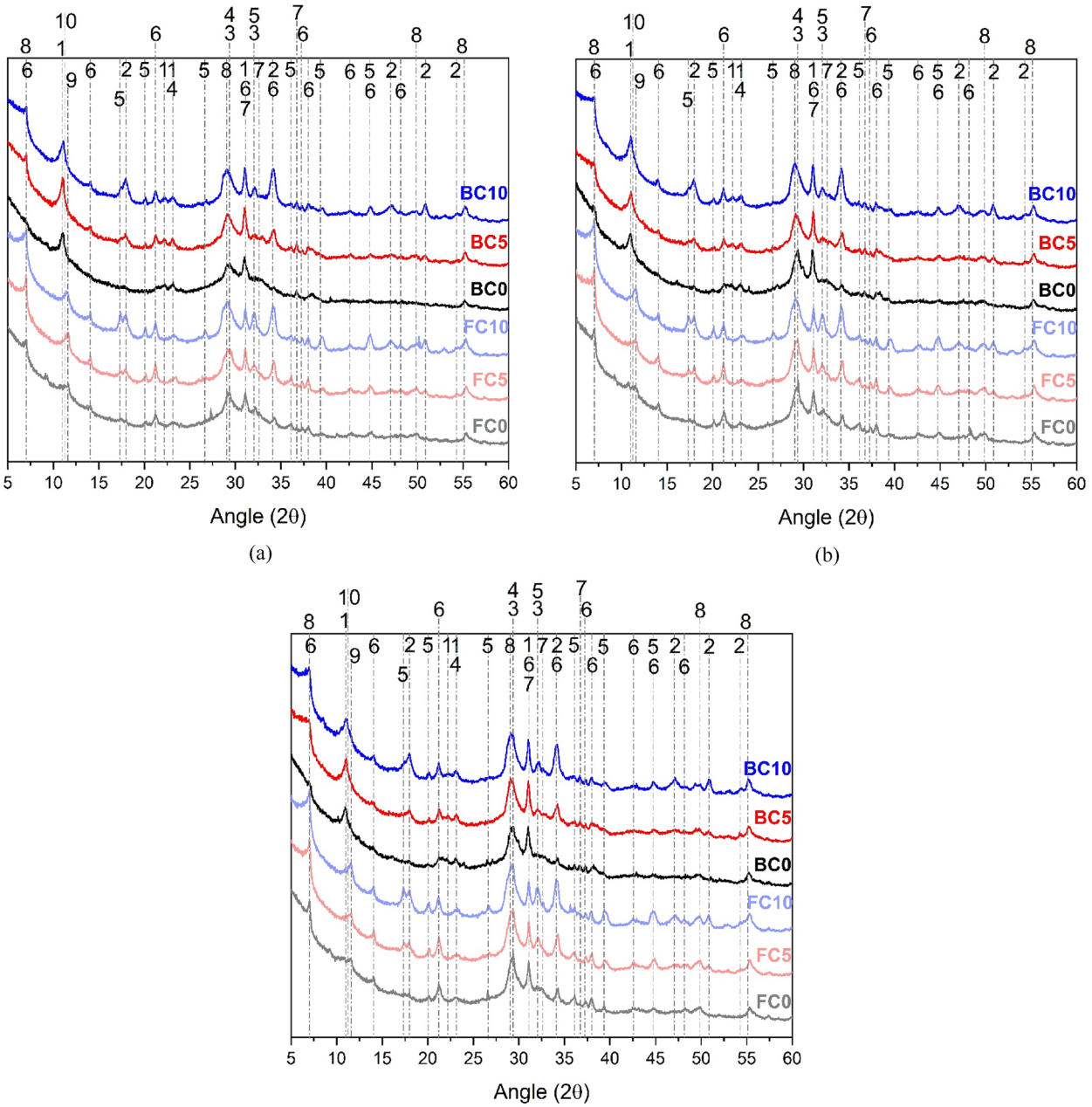

Fig. 3 Hydration reactants at curing ages, (**a**) 1d, (**b**) 7d, (**c**) 28d. 1: Friedel's salt, 2: portlandite, 3: CSH gel, 4: calcite, 5: C3AH6, 6: C2ASH8, 7: C4AH13, 8: CSH(I), 9: monocarboaluminate, 10: hydrotalcite

$M = MgO$, $S = SiO_2$, $A = Al_2O_3$, $C = CaO$, $\$ = SO_3$, $H = H_2O$, $\underline{C} = CO_2$).

$$C_4AH_{13} \rightarrow 2C_3AH_6 + 9H \quad (2)$$

$$2C_3A + 21H \rightarrow C_2AH_8 + C_4AH_{13} \rightarrow 2C_3AH_6 + 9H \quad (3)$$

$$C_2S + AH_3 + 5H \rightarrow C_2ASH_8 \quad (4)$$

$$\underline{C} + CH \rightarrow C\underline{C} + H \quad (5)$$

$$C_3A + C\underline{C} + 11H \rightarrow C_4A\underline{C}H_{11} \quad (6)$$

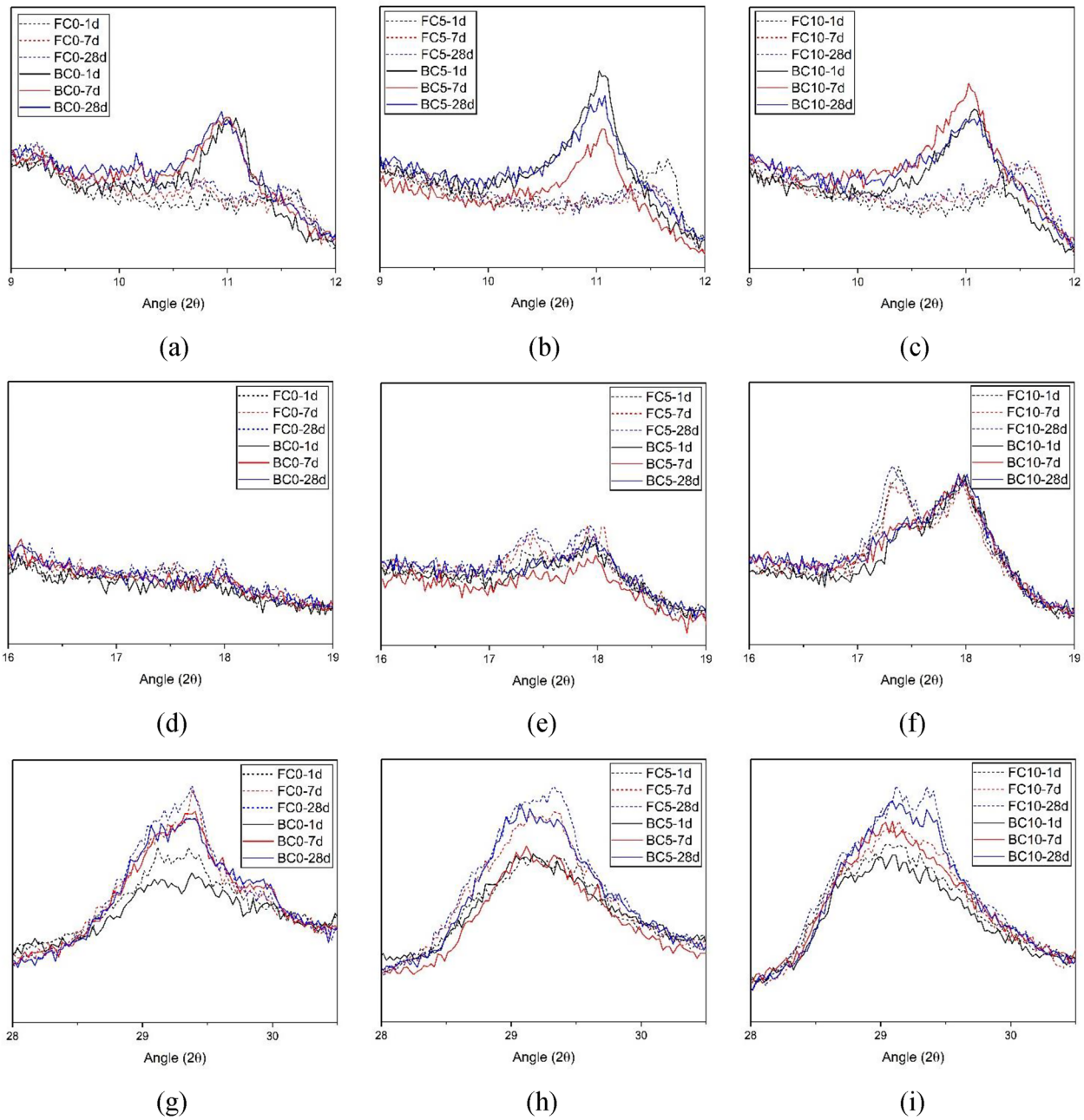

Fig. 4 Partial magnification in XRD analysis (in Fig. 3), (**a**) 9–12° range, 0% CH, (**b**) 9–12° range, 5% CH, (**c**) 9–12° range, 10% CH, (**d**) 16–19° range, 0% CH, (**e**) 16–19° range, 5% CH, (**f**) 16–19° range, 10% CH, (**g**) 28–30.5° range, 0% CH, (**h**) 28–30.5° range, 5% CH, (**i**) 28–30.5° range, 10% CH

$$C_{12}A_7 + 9Ca^{2+} + C\underline{C} + 11H \rightarrow C_4A\underline{C}H_{11} \quad (7)$$

$$2C_2S + 4H \rightarrow C_3S_2H_3 + CH \quad (8)$$

$$2C_3S + 6\,H \rightarrow C_3S_2H_3 + 3CH \quad (9)$$

$$M_6A + 12H + \underline{C} \rightarrow M_6A\underline{C}H_4 + 4H \quad (10)$$

$$C_3A + CaCl_2 + 10H \rightarrow C_4ACl_2H_{10} \quad (11)$$

$$3CH + CaCl_2 + A + 7H \rightarrow 3C_4ACl_2H_{10} \quad (12)$$

Peak intensity difference analysis of the hydration phase through XRD analysis shows the change in the relative hydration phase of the BC and FC specimens. However, through Figs. 3 and 4, only the types and phases of

hydration reactants by BC and FC can be known. In the next section, Sect. 3.3, we will examine the specific phase change through thermal analysis.

3.3 Thermal Analysis

Fig. 5 shows the results of thermal analysis (TG/DTA). Weight loss in the 30–100 °C range is due to evaporation of free water. And in the temperature range of 50–200 °C, CSH (50–200 °C) (Ben Haha et al., 2011), CSH(I) (90–110 °C) (Jambunathan et al., 2013), C4AH13(125 °C) (Zhu et al., 2012), CAH10 (85–105 °C) (Son et al., 2018), C2ASH8 (175–185 °C) (Ghadikolaee et al., 2021) and monocarboaluminate (90–150 °C) (Jambunathan et al., 2013) show weight loss according to decomposition. Weight loss due to decomposition of AH3 was observed in the temperature range of 230–300 °C (Montes et al., 2018). C3AH6 was observed in the range of 240–370 °C (Antonovič et al., 2013), and weight loss due to the decomposition of Friedel's salt was observed in the range of 230–370 °C (Wang et al., 2019c; Zhang et al., 2019). Weight loss due to decomposition of portlandite was measured in the temperature range of 400–500 °C (Matúš et al., 2015). The weight loss in the wide range of 550–800 °C is due to the decomposition of calcite (Shi et al., 2017a, 2017b; Villain et al., 2007).

The weight loss due to the decomposition of C4AH13 observed at 125 °C was greater for RC specimens than for TC. As mentioned in the XRD analysis, this shows a result consistent with the fact that the C4AH13 peak intensity of the BC specimens was greater than that of the FC. In addition, the temperature range of 230–300 °C is the weight loss due to the decomposition of AH3, and the FC specimens showed a greater reduction rate than BC. Amorphous AH3 was not detected in the XRD analysis results. The weight loss of AH3 showed a greater weight loss rate as the concentration of CH increased. As a result, the weight loss rate of the BC specimens was smaller than that of FC because AH3 reacted with CH to form a hydration product containing aluminum such as Freidel's salt or monocarboaluminate. In the temperature range of 230–370 °C, the weight loss due to the decomposition of the three phases of AH3, C3AH6 and Friedel's salt was measured simultaneously. As expected, the portlandite in the temperature range of 400–500 °C increased as the concentration of CH increased in both BC and FC specimens. Compared to the 0% CH specimen (black dash line and brown solid line), the weight reduction effect of portlandite can be clearly confirmed.

Table 5 shows the weight loss rate for each temperature region representing the hydration reactant.

In Table 5, the weight loss in the temperature range of 30–200 °C was 28 d greater than 1 d at all CH concentrations. This means that the generation of hydration reactants increased with time. Except for 0% CH at 1d, the weight loss rate at each CH concentration and age was greater in BC specimens. This means that brine promotes hydration of slag more than fresh water.

The weight loss in the range of 230–400 °C overlaps with the weight loss effect due to the decomposition of AH3, C3AH6 and Friedel's salt. At 1 d of 0% CH, the decrease rate was FC of 10.22%, which was greater than BC's 9.62%. However, in the remaining CH concentrations and ages, the weight loss rate of the BC specimen was greater than that of the FC. This means that the formation of the main hydration reactant phase increased more in BC than in FC.

In the temperature range of 400–500 °C, FC, a fresh water test, showed a greater weight loss than BC at all CH concentrations and ages. It is believed that the relatively increased consumption of portlandite in BC is

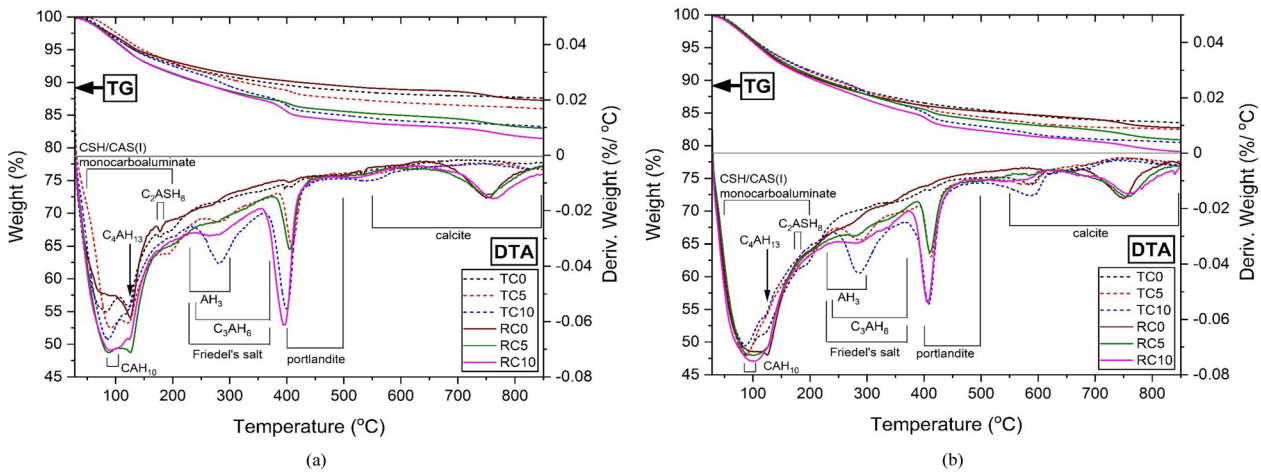

Fig. 5 Thermal analysis, (**a**) 1d, (**b**) 28d

Table 5 Mass loss percentages from TG analysis

Mix water	CH (wt.%)	Age (day)	Temperature range (℃)				
			30–200[1)]	30–400[2)]	400–500[3)]	550–800[4)]	Total weight loss (30–850)
Fresh water	0%	1	6.99	10.22	0.83	0.70	12.21
		28	9.08	13.34	1.04	1.36	16.38
	5%	1	7.11	11.37	1.25	1.02	14.20
		28	8.68	13.96	1.64	1.28	17.52
	10%	1	7.45	13.48	1.53	1.04	16.74
		28	8.36	14.79	2.11	1.73	19.40
Brine	0%	1	6.61	9.62	0.79	1.61	12.60
		28	9.20	13.65	0.88	2.03	17.07
	5%	1	8.60	13.06	1.27	1.96	16.92
		28	8.99	14.30	1.64	2.30	18.97
	10%	1	8.42	14.25	1.42	1.93	18.43
		28	9.47	15.46	2.02	2.38	20.72

[1)]30–200: free water, CSH, CSH(I), C4AH13, CAH10, C2ASH8, monocarboaluminate, [2)]30–400: 30–200 phases + AH3, Friedel's salt, C3AH6, [3)]400–500: portlandite, [4)]550–800: calcite

because it is consumed in the formation of hydration reactants with ions supplied from brine such as Friedel's salt.

At 550–800 °C, the weight loss due to the decomposition of calcite was shown, and the BC test specimens showed a larger value than the FC. The reason why the calcite phase of the BC specimens was more than that of the FC was as follows. The increase in calcite in the brine sample may be due to decomposition by carbonation of Friedel's salt by reacting with atmospheric carbon dioxide (Anstice et al., 2005; Ke et al., 2017). C3AH6 has higher carbonation resistance than Friedel's salt (Plank et al., 2016). Therefore, the calcite phase is relatively low in the FC specimen, which is rich in C3AH6 phase and free of Friedel's salt.

The total weight loss rate in the entire temperature range of 30–850 °C was higher in BC specimens than in FC at all CH concentrations and ages. In view of these results, it is judged that brine promotes the hydration of slag, and CH has a synergistic effect of improving the hydration reaction of brine.

Fig. 6 shows portlandite content and chemically bound water (CBW) calculated from the thermal analysis data in Fig. 5. Each value was calculated by Eq. (13) (Shi et al., 2017a, 2017b) and Eq. (14) (Sun et al., 2022).

$$m_{ch} = \frac{M_{ch}}{M_w} \times m \tag{13}$$

Here, m_{ch} is the mass of fraction (wt%) of portlandite in the sample, M_{ch} is the molar mass of portlandite, and M_w is the molar mass of water (H_2O). And m refers to the weight loss (tangential method) value in the temperature range of 400–500 °C in the thermal analysis data in Fig. 5.

$$\mathrm{CBW} = \frac{m_{50} - m_{550}}{m_{550}} \times 100(\%) \tag{14}$$

where m_{50} and m_{550}, MA, and MB represent the remaining weights of the sample when the temperature reaches 50 and 550 °C, respectively.

In Fig. 6a, at all CH contents, brine specimens showed lower portlandite content fraction than FC spceimens at 1d and 28d. This is because brine promoted the hydration reaction of slag and increased the production of hydration product (Jun et al., 2021; Kang & Kim, 2020). Additionally, compared to FC, additional portlandite was consumed in the formation of Friedel's salt due to the mixing of brine, and a relatively smaller portlandite content fraction than FC was observed. This acceleration of the formation of hydration reactants resulted in improved mechanical performance of specimens using brine rather than FC. Fig. 6b shows the strength characteristics for the content of chemically bound water. At 0% CH, brine specimens show lower chemically bound water values than FC. A relatively higher chemically bound water content means the formation of more hydration reactants (Sun et al., 2022). Therefore, this means that the FC test specimen had more hydration reaction products than brine, and as mentioned previously in Fig. 2a, the strength was higher than that of brine when FC was 1d and 28d. However, at 5 and 10% CH, the brine specimens

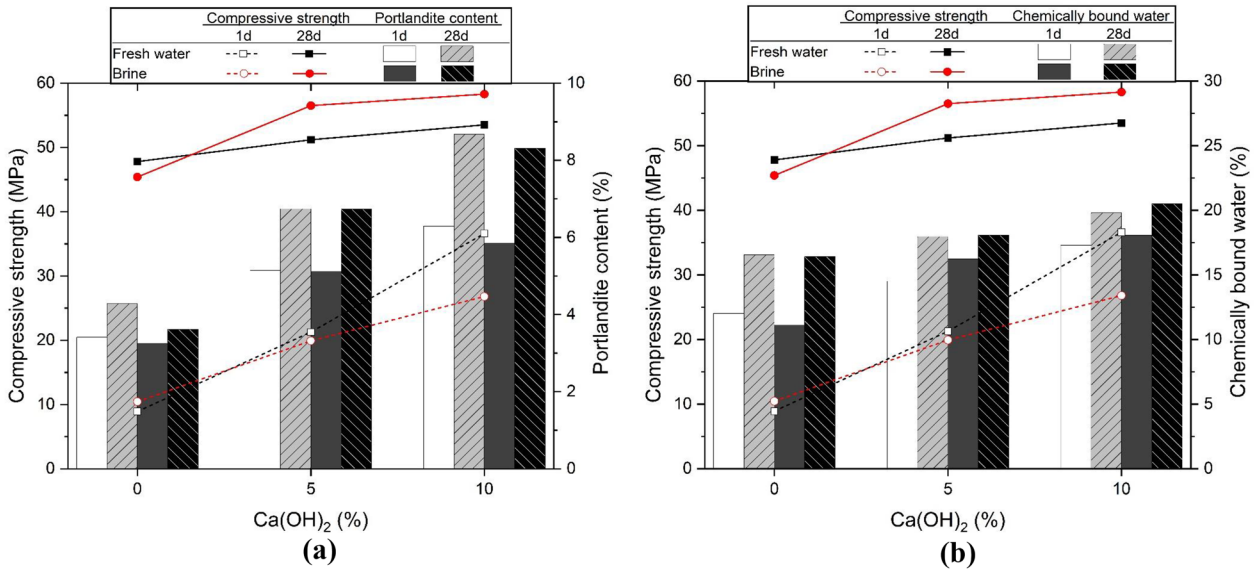

Fig. 6 Correlation between compressive strength, portlandite content, and chemically bound water (**a**) portlandite content, (**b**) chemically bound water

showed a higher chemically bound water content than FC. This means that the brine test specimens showed higher compressive strength than FC at both 1d and 28d. As a result, specimens using brine as a mixing water promote the hydration reaction of the slag, forming more hydration products, which leads to an improvement in compressive strength.

3.4 FT–IR

Fig. 7 shows the FT–IR analysis results. The weak peaks observed at 426, 524 and 786 cm^{-1} are attributed to the AlO_6 octahedra, confirming the presence of the Friedel's salt phase (Shao et al., 2013). In the FT–IR of the BC specimens, peak deflection and change are clearly observed, but the FC specimens do not appear, and the difference in the hydration reactants of the two specimens is clearly distinguished.

Assigned to the Si–O stretch at 959 cm^{-1} (range 900–1000 cm^{-1}) (Shao et al., 2013; Ylmén & Jäblid 2013), we see the presence of a CSH phase. At 1d, a larger and clearer peak near 959 cm^{-1} of the brine specimens can be identified, which is believed to increase the formation of CSH, a hydration reactant, by promoting the hydration reaction of the slag. However, at 28d, similar peak changes were observed in BC and FC specimens. This means that the hydration reaction of slag proceeds gradually over time, and as a result, brine has a greater effect on the hydration reaction of slag in the early–age of 1d.

In addition, in the peaks of 450 and 669 cm^{-1}, absorption bands due to the vibration of the Si–O bond and the Al–O vibration of the AlO group were observed, indicating that the CASH phase was formed (Song et al., 2021). It is observed in both BC and FC specimens, which is thought to be due to the mixing of Al_2O_3. The 669 cm^{-1} peak indicates the formation of a monocarboaluminate phase (Horgnies et al., 2013) or the presence of a C4AH13 phase (Horgnies et al., 2013).

Peaks at 450 and 1050 cm^{-1} were observed due to the absorption bands of Si–O and Al–O related to the presence of the C2ASH8 phase (Horgnies et al., 2013). It is observed at 1d and 28d in FC specimens and BC specimens.

Peaks observed at 716, 852, 875, 1425 and 1473 cm^{-1} confirm the presence of calcite phases (Ylmén & Jäblid 2013; Choudhary et al., 2015; Trezza & Lavat, 2001; Liu et al., 2022) due to the asymmetric stretching of CO_3^{2-}. The 1363 cm^{-1} peak is due to the stretching vibration of CO_3^{2-} and means the formation of monocarboaluminate phase (Horgnies et al., 2013). In the XRD analysis in Fig. 3, the FC specimens showed a clearer monocarboaluminate peak than the BC specimens. This is confirmed by the fact that the gradual curvature change of the absorption band observed at 1363 cm^{-1} is better observed in FC specimens.

The 1600–1700 cm^{-1} range (including the 1650 cm^{-1} peak) and the 3100–3400 cm^{-1} region confirm the presence of water molecules due to the symmetric and asymmetric stretching vibrations of O–H (Lemougna et al., 2017; Trezza, 2007).

The peak observed at 3643 cm^{-1} is due to the stretching vibration of O–H, indicating the formation of the CH

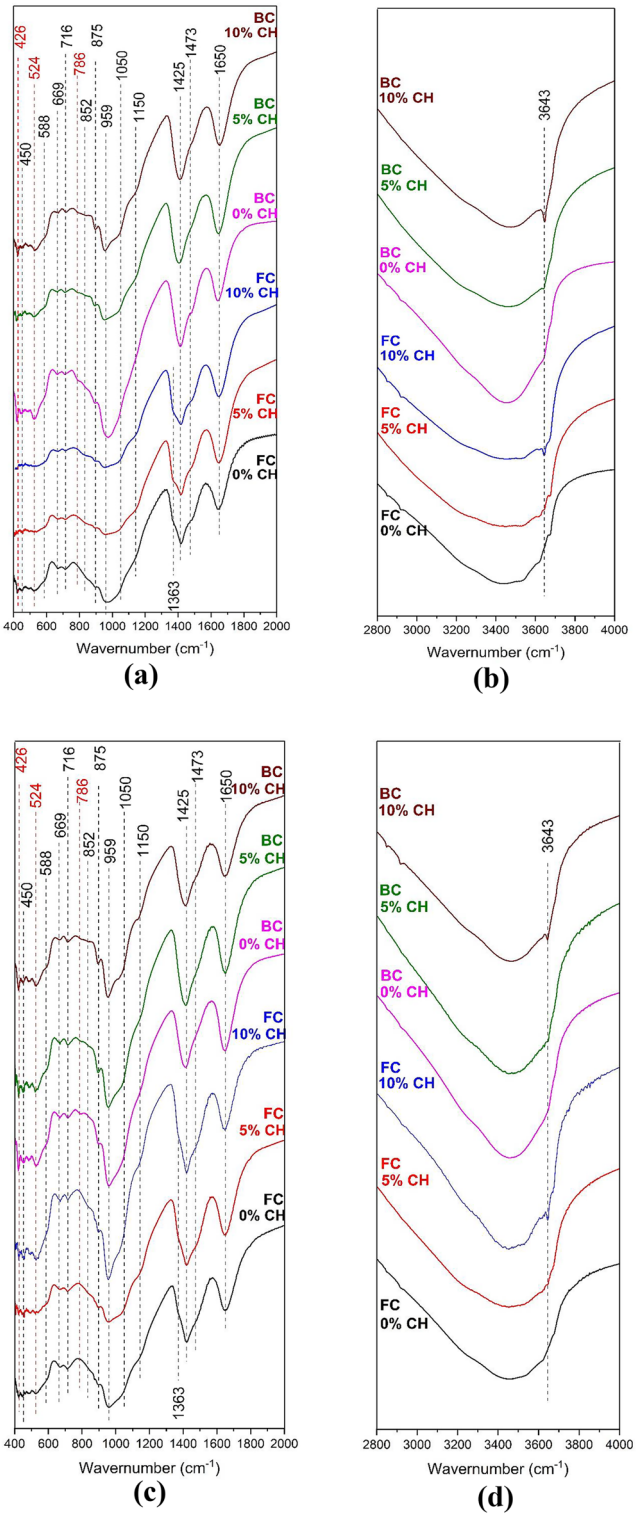

Fig. 7 FT–IR analysis, (**a**) 1d, 400–200 cm^{-1} range, (**b**) 1d, 2800–4000 cm^{-1} range, (**c**) 28d, 400–200 cm^{-1} range, (**d**) 28d, 2800–4000 cm^{-1} range (*FC* fresh water, *BC* brine, CH: $(Ca(OH)_2)$

phase (Horgnies et al., 2013; Ylmén et al., 2009). The size of the 3643 cm^{-1} peak was clearly sharp and increased with increasing CH concentration in both FC and BC specimens. Therefore, the 10% CH specimens confirm the presence of the sharpest peak.

3.5 Microstructures

Fig. 8 shows each sample's SEM images at 28d. The FC samples (Fig. 8a–c) and brine samples (Fig. 8d, e) show a dense hydration reactant matrix. The energy dispersive X-ray spectrometer (EDS) analysis was performed on the

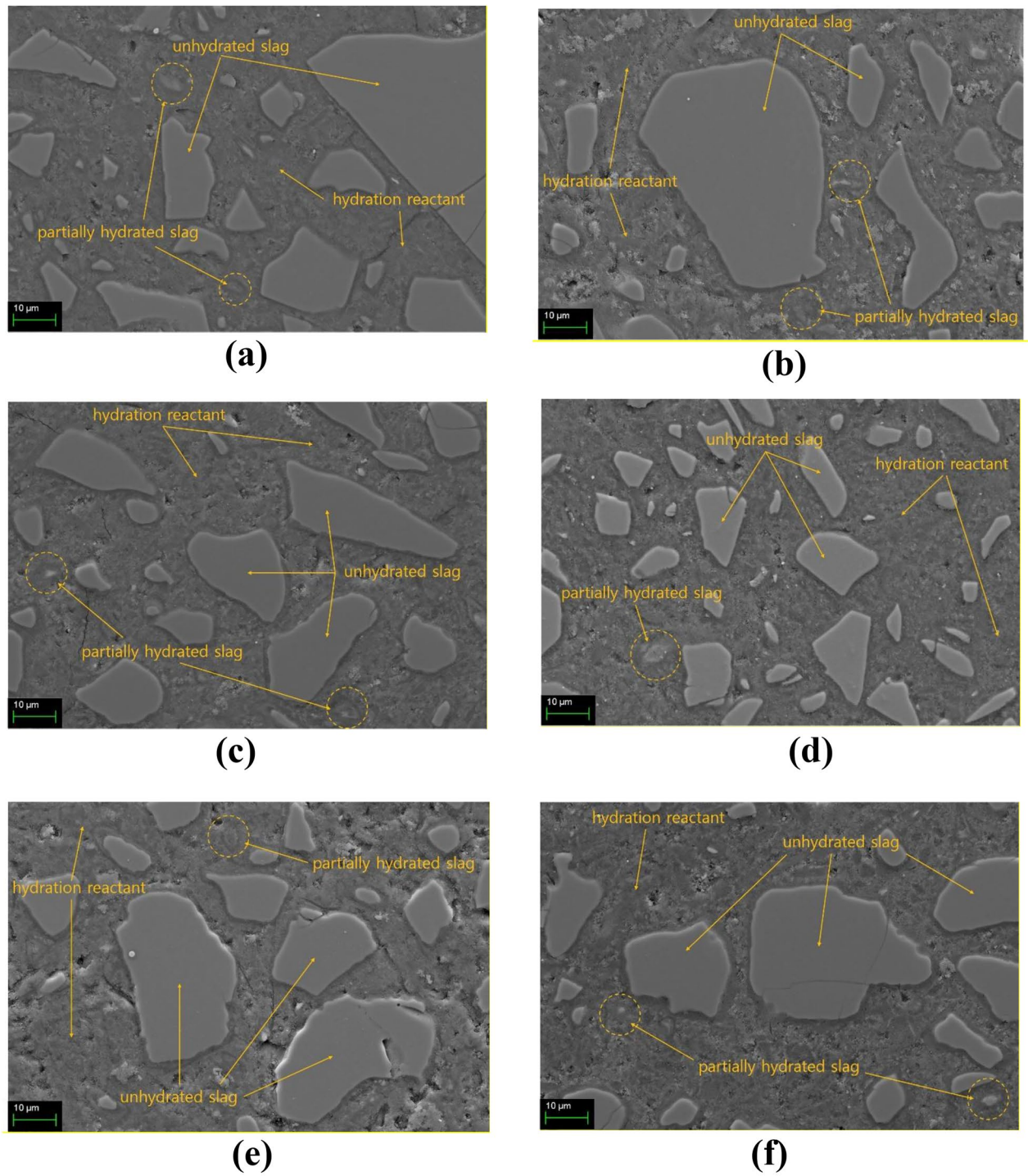

Fig. 8 SEM images, (**a**) FC0, (**b**) FC5, (**c**) FC10, (**d**) BC0, (**e**) BC5, and (**f**) BC10

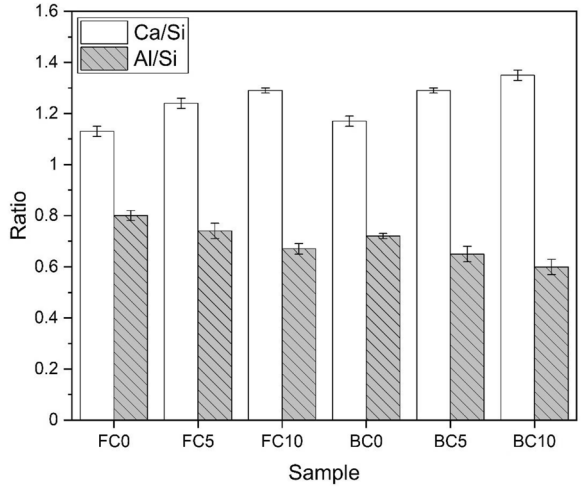

Fig. 9 EDS analysis results for hydration reactants

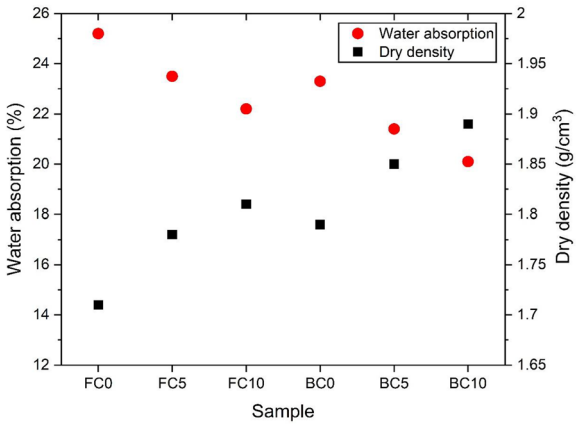

Fig. 10 Water absorption and dry density

hydration reactants formed around the unhydrated slag particles in Fig. 8. The EDS analysis was conducted on 15 points random hydration reactants, and the average value was calculated. The measured values are shown in Fig. 9. In the FC and brine samples, as CH increased, the amount of Ca/Si increased while that of Al/Si decreased. The brine samples had higher Ca/Si and lower Al/Si than FC. This is assumed to be due to the promotion of slag hydration of brine and the supply of calcium ions by CH. Research results indicating that seawater promotes the hydration reaction of slag support this fact (Jun et al., 2020; Kang & Kim, 2020). The increase of CSH gel in Ca/Si, a representative hydration reaction of slag, improves the physical adsorption capacity of chloride ions (Plusquellec & Nonat, 2016; Yang et al., 2019; Zhou et al., 2016). It is one of the critical factors that affect the chloride ion adsorption capacity of the brine samples. Therefore, it can be expected that adding CH could improve the ability of the CSH gel to adsorb chloride ions when brine is used as mix water.

3.6 *Water–Absorption and Density*

Fig. 10 shows the water–absorption rate and dry density measurements of the 28 d specimens. The water–absorption rate in 10% CH specimens was lowest of the FC and BC samples. Next, for the 5% CH specimens; the highest absorption was for 0% CH specimens. Dry density also showed a similar tendency for water absorption. It implies that the density values decreased in the order of 10% CH > 5% CH > 0% CH specimens in FC and brine. The 10% CH samples showed the lowest absorption rate and the highest density regardless of the FC or BC mix water.

Low absorption and high density mean that the internal matrix of the specimen is dense, and consequently, the mechanical performance is improved. As mentioned in the compressive strength results in Fig. 1, 10% CH showed the highest strength value.

The mixture of CH and brine promotes the formation of hydration reactants and densifies the matrix, which is believed to exert a synergistic effect on improving mechanical performance. This can be clearly confirmed by the fact that, compared to the 0% CH test specimen, the mixture of CH showed a higher density, lower water absorption and higher compressive strength (see Fig. 1) under the condition that the same brine was used as the mixing water.

4 Conclusion

The effects of brine (BC) and clacium hydroxide ($Ca(OH)_2$: CH) on the hydration process of slag were investigated. In addition, the characteristics and effects were compared with fresh water (FC) specimens. A summary of the experimental and analytical results is as follows.

1. Specimens without CH (only with aliminum oxide(AO)) have very low compressive strength in the initial 1d and 3d stages. Compared to CH, AO had a very low activation effect of slag. However, the use of CH enhances the early strength by accelerating the activation reaction of slag. A mixture with only AO and no CH showed a sharp increase in strength at 7 days. This means that a long time is required for AO to show an effect on the hydration reaction of slag. BC specimens showed improved mechanical performance over FC at all ages and mixes. Therefore, it was shown that the slag-AO-CH combination

can secure sufficient mechanical performance as a construction material.

2. FC samples formed more C3AH6 phase than brine. As the metastable phases, CAH10 and C4AH13, are converted to the stable phase C3AH6, the mechanical properties are reduced due to volume instability. Consequently, the compressive strength of FC samples was reduced when compared to brine. The brine samples produced more calcite phase than FC. CH and brine affect the mechanical properties by changing the type and phase of the hydration reactants.
3. The hydration reaction product of slag activated with CH and AO exhibited a dense structure. According to the results of the EDS analysis of hydration reactants, an increase in the amount of CH increased Ca/Si and decreased Al/Si. It is considered that brine promotes slag hydration and improves the dissolution of the active ingredient. The brine sample had higher Ca/Si values than the FC, which means that the chloride ion adsorption capacity of the samples using brine as the mix water was improved.
4. According to the density and absorption rate measurement results, in the 10% CH sample, the increase in absorption rate and decrease in density is due to cracking caused by excessive expansion at high temperature (60 °C) curing. These results explain why the 10% CH samples showed lower compressive strength than 5% CH. When using AO as an activator and brine as mix water, improving the mechanical properties is advantageous if CH does not exceed 10%.

This study confirms the feasibility of using brine as a building material. As confirmed in the experimental results, the effect of the combined mixture of slag-brine-$Ca(OH)_2$ on the properties of the hydration reaction and mechanical performance was confirmed. The results of this study are expected to further expand the possibility of using brine for manufacturing construction materials.

Author contributions

CK: validation, formal analysis, investigation, supervision, methodology, experimentation, writing original/final draft. TK: project administration, conceptualization, validation, formal analysis, experimentation, writing original/final draft and writing review/editing. YP: conceptualization, formal analysis, validation, writing review/editing. KS: validation, methodology, investigation, formal analysis. All authors read and approved the final manuscript. All authors contributed to the paper.

Funding

This work was supported by the National Research Foundation of Korea(NRF) grant funded by the Korea Government(MOE) (NRF-2020R1I1A1A01056497).

Availability of data and materials

The data sets used and analyzed during the current study are available from the corresponding author upon reasonable request.

Competing interests

The authors declare that they have no competing interests.

Received: 28 July 2023 Accepted: 11 March 2024
Published online: 24 June 2024

References

Anstice, D. J., Page, C. L., & Page, M. M. (2005). The pore solution phase of carbonated cement pastes. *Cement and Concrete Research, 35*, 377–383. https://doi.org/10.1016/j.cemconres.2004.06.041

Antonovič, V., Kerienė, J., Boris, R., & Aleknevičius, M. (2013). The effect of temperature on the formation of the hydrated calcium aluminate cement structure. *Procedia Engineering, 57*, 99–106. https://doi.org/10.1016/j.proeng.2013.04.015

ASTM-C1403. (2022). *Standard test method for rate of water absorption of masonry mortars*. West Conshohocken: American Society for Testing and Materials.

ASTM-C305. (2020). *Standard practice for mechanical mixing of hydraulic cement pastes and mortars of plastic consistency*. West Conshohocken: American Society for Testing and Materials.

Ben Haha, M., Le Saout, G., Winnefeld, F., & Lothenbach, B. (2011). Influence of activator type on hydration kinetics, hydrate assemblage and microstructural development of alkali activated blast-furnace slags. *Cement and Concrete Research, 41*(3), 301–310. https://doi.org/10.1016/j.cemconres.2010.11.016

Chang, H. (2017). Chloride binding capacity of pastes influenced by carbonation under three conditions. *Cement and Concrete Composites, 84*, 1–9. https://doi.org/10.1016/j.cemconcomp.2017.08.011

Chang, H., Feng, P., Lyu, K., & Liu, J. (2019). A novel method for assessing C-S-H chloride adsorption in cement pastes. *Construction and Building Materials, 225*, 324–331. https://doi.org/10.1016/j.conbuildmat.2019.07.212

Chang, L., Liu, H., Wang, J., Liu, H., Song, L., Wang, Y., & Cui, P. (2022). Effect of chelation via ethanol-diisopropanolamine on hydration of pure steel slag. *Construction and Building Materials, 357*, 129372. https://doi.org/10.1016/j.conbuildmat.2022.129372

Chen, P., Ma, B., Tan, H., Liu, X., Zhang, T., Qi, H., Peng, Y., Yang, Q., & Wang, J. (2020). Effects of amorphous aluminum hydroxide on chloride immobilization in cement-based materials. *Construction and Building Materials, 231*, 117171. https://doi.org/10.1016/j.conbuildmat.2019.117171

Choudhary, H. K., Anupama, A. V., Kumar, R., Panzi, M. E., Matteppanavar, S., Sherikar, B. N., & Sahoo, B. (2015). Observation of phase transformations in cement during hydration. *Construction and Building Materials, 101*, 122–129. https://doi.org/10.1016/j.conbuildmat.2015.10.027

De Weerdt, K., Colombo, A., Coppola, L., Justnes, H., & Geiker, M. (2015). Impact of the associated cation on chloride binding of Portland cement paste. *Cement and Concrete Research, 68*, 196–202. https://doi.org/10.1016/j.cemconres.2014.01.027

Duran, A., Sirera, R., Pérez-Nicolás, M., Navarro-Blasco, I., Fernández, J. M., & Alvarez, J. I. (2016). Study of the early hydration of calcium aluminates in the presence of different metallic salts. *Cement and Concrete Research, 81*, 1–15. https://doi.org/10.1016/j.cemconres.2015.11.013

Fan, X., Wang, Y., Yu, Q., Gao, X., Ye, J., & Zhang, Y. (2023). Improving the chloride binding capacity of alkali activated slag by calcium and aluminum enriched minerals. *Journal of Building Engineering, 70*, 106384. https://doi.org/10.1016/j.jobe.2023.106384

Galan, I., & Glasser, F. P. (2015). Chloride in cement. *Advances in Cement Research., 27*(2), 63–97. https://doi.org/10.1680/adcr.13.00067

Gbozee, M., Zheng, K., He, F., & Zeng, X. (2018). The influence of aluminum from metakaolin on chemical binding of chloride ions in hydrated cement pastes. *Applied Clay Science, 158*, 186–194. https://doi.org/10.1016/j.clay.2018.03.038

Ghadikolaee, M. R., Korayem, A. H., Sharif, A., & Liu, Y. M. (2021). The halloysite nanotube effects on workability, mechanical properties, permeability and microstructure of cementitious mortar. *Construction and Building Materials, 267*, 120873. https://doi.org/10.1016/j.conbuildmat.2020.120873

Horgnies, M., Chen, J. J., & Bouillon, C. (2013). Overview about the use of fourier transform infrared spectroscopy to study cementitious materials. *WIT*

Transactions on Engineering Sciences, 77, 251–262. https://doi.org/10.2495/MC130221

Hussain, S. E., & Al-Saadoun, S. (1990). Effect of tricalcium aluminate content of cement on chloride binding corrosion of reinforcing steel in concrete. *Cement and Concrete Research, 20*(1), 723–738. https://doi.org/10.1016/0008-8846(90)90006-J

Jambunathan, N., Sanjayan, J. G., Pan, Z., Li, G., Liu, Y., Korayem, A. H., Duan, W. H., & Collins, F. (2013). The role of alumina on performance of alkali-activated slag paste exposed to 50 ºC. *Cement and Concrete Research, 54*, 143–150. https://doi.org/10.1016/j.cemconres.2013.09.009

Janotka, I. (2001). Hydration of the cement paste with Na_2CO_3 addition. *Ceramics Silikáty, 45*(1), 16–23.

Jin, H., Li, Z., Zhang, W., Liu, J., Xie, R., Tang, L., & Zhu, L. (2022). Iodide and chloride ions diffusivity, pore characterization and microstructures of concrete incorporating ground granulated blast furnace slag. *Journal of Materials Research and Technology, 16*, 302–321. https://doi.org/10.1016/j.conbuildmat.2021.122561

Jin, H., Liu, J., Jiang, Z., Zhou, H., & Liu, J. (2021). Influence of the rainfall intensity on the chloride ion distribution in concrete with different levels of initial water saturation. *Construction and Building Materials, 281*, 122561. https://doi.org/10.1016/j.conbuildmat.2021.122561

Jones, E., Qadir, M., van Vliet, M. T. H., Smakhtin, V., & Kang, S.-M. (2019). The state of desalination and brine production: a global outlook. *Science of The Total Environment, 657*, 1343–1356. https://doi.org/10.1016/j.scitotenv.2018.12.076

Jun, Y., Kim, J. H., Han, S. H., & Kim, T. (2021). Influence of seawater on alkali-activated slag concrete. *Materials and Structures, 54*(3), 121. https://doi.org/10.1617/s11527-021-01719-5

Jun, Y., Kim, T., & Kim, J. H. (2020). Chloride-bearing characteristics of alkali-activated slag mixed with seawater: effect of different salinity levels. *Cement and Concrete Composites, 112*, 103680. https://doi.org/10.1016/j.cemconcomp.2020.103680

Kang, C., & Kim, T. (2020). Pore and strength characteristics of alkali-activated slag paste with seawater. *Magazine of Concrete Research, 72*(10), 199–508. https://doi.org/10.1680/jmacr.18.00390

Kang, C., & Kim, T. (2023). Influence of brine on hydration reaction of calcium sulfoaluminate and slag blended cement. *Case Studies in Construction Materials, 18*, e02159. https://doi.org/10.1016/j.cscm.2023.e02159

Ke, X., Bernal, S. A., & Provis, J. L. (2017). Uptake of chloride and carbonate by Mg-Al and Ca-Al layered double hydroxides in simulated pore solutions of alkali-activated slag cement. *Cement and Concrete Research, 100*, 1–13. https://doi.org/10.1016/j.cemconres.2017.05.015

Koch, M. S., Schopmeyer, S. A., Nielsen, O. I., Kyhn-Hansen, C., & Madden, C. J. (2007). Conceptual model of seagrass die-off in florida bay: links to biogeochemical processes. *Journal of Experimental Marine Biology and Ecology, 350*, 73–88. https://doi.org/10.1016/j.jembe.2007.05.031

Lemougna, P. N., Wang, K.-T., Tang, Q., & Cui, X.-M. (2017). Study on the development of inorganic polymers from red mud and slag system: application in mortar and lightweight materials. *Construction and Building Materials, 156*, 486–495. https://doi.org/10.1016/j.conbuildmat.2017.09.015

Li, C., Li, G., Chen, D., Gao, K., Mao, Y., Fan, S., Tang, L., & Jia, H. (2023). Influencing mechanism of nano-Al_2O_3 on concrete performance based on multi-scale experiments. *Construction and Building Materials, 384*, 131402. https://doi.org/10.1016/j.conbuildmat.2023.131402

Li, C., Song, X., & Jiang, L. (2021). A time-dependent chloride diffusion model for predicting initial corrosion time of reinforced concrete with slag addition. *Cement and Concrete Research, 145*, 106455. https://doi.org/10.1016/j.cemconres.2021.106455

Li, H., Tang, Z., Li, N., Gui, L., & Mao, X. (2020). Mechanism and process study on steel slag enhancement for CO2 capture by seawater. *Applied Energy, 276*, 115515. https://doi.org/10.1016/j.apenergy.2020.115515

Liu, J., Fan, X., Liu, J., Jin, H., Zhu, J., & Liu, W. (2021). Investigation on mechanical and micro properties of concrete incorporating seawater and sea sand in carbonized environment. *Construction and Building Materials, 307*, 124986. https://doi.org/10.1016/j.conbuildmat.2021.124986

Liu, T., Yu, Q., & Brouwers, H. J. H. (2022). In-situ formation of layered double hydroxides (LDHs) in sodium aluminate activated slag: the role of Al–O tetrahedral. *Cement and Concrete Research, 153*, 106697. https://doi.org/10.1016/j.cemconres.2021.106697

Liu, X., Maa, B., Tan, H., Li, H., Mei, J., Zhang, T., Chen, P., & Gu, B. (2019). Chloride immobilization of cement-based material containing nano-Al2O3. *Construction and Building Materials, 220*, 43–52. https://doi.org/10.1016/j.conbuildmat.2019.05.148

Matúš, Ž, Eva, K., Marta, K., Jakub, T., & Martin, P. (2015). Study of hydration products in the model systems metakaolin-lim and metakaolin-lim-gypsum. *Ceramics Silikáty, 59*(4), 283–291.

Montes, M., Pato, E., Carmona-Quiroga, P. M., & Blanco-Varela, M. T. (2018). Can calcium aluminates activate ternesite hydration? *Cement and Concrete Research, 103*, 204–215. https://doi.org/10.1016/j.cemconres.2017.10.017

Morsy, M. S. (2005). Effect of temperature on hydration kinetics and stability of hydration phases of metakaolin-lime sludge-silica fume system. *Ceramics Silikáty, 49*(4), 225–229.

Nazari, A., & Riahi, S. (2011). Improvement compressive strength of concrete in different curing media by Al2O3 nanoparticles. *Materials Science and Engineering: A, 528*, 1183–1191. https://doi.org/10.1016/j.msea.2010.09.098

Ortega, J. M., Sanchez, I., & Climent, M. A. (2012). Durability related transport properties of OPC and slag cement mortars hardened under different environmental conditions. *Construction and Building Materials, 27*, 176–183. https://doi.org/10.1016/j.conbuildmat.2011.07.064

Palin, D., Jonkers, H. M., & Wiktor, V. (2016). Autogenous healing of sea-water exposed mortar: quantification through a simple and rapid permeability test. *Cement and Concrete Research, 84*, 1–7. https://doi.org/10.1016/j.cemconres.2016.02.011

Panagopoulos, A., Haralambous, K.-J., & Loizidou, M. (2019). Desalination brine disposal methods and treatment technologies—a review. *Science of The Total Environment, 693*, 133545. https://doi.org/10.1016/j.scitotenv.2019.07.351

Plank, J., Zhang-Preße, M., Ivleva, N. P., & Niessner, R. (2016). Stability of single phase C3A hydrates against pressurized CO_2. *Construction and Building Materials, 122*, 426–434. https://doi.org/10.1016/j.conbuildmat.2016.06.042

Plusquellec, G., & Nonat, A. (2016). Interactions between calcium silicate hydrate (C-S-H) and calcium chloride, bromide and nitrate. *Cement and Concrete Research, 90*, 89–96. https://doi.org/10.1016/j.cemconres.2016.08.002

Portillo, E., de la Ruiz Rosa, M., Louzara, G., Quesada, J., Ruiz, J. M., & Mendoza, H. (2014). Dispersion of desalination plant brine discharge under varied hydrodynamic conditions in the south of Gran Canaria. *Desalination and Water Treatment, 52*, 164–177. https://doi.org/10.1080/19443994.2013.795349

Pruckner, F., & Gjørv, O. (2004). Effect of CaCl2 and NaCl additions on concrete corrosivity. *Cement and Concrete Research, 34*, 1209–1217. https://doi.org/10.1016/j.cemconres.2003.12.015

Qasim, M., Badrelzaman, M., Darwish, N. N., Darwish, N. A., & Hilal, N. (2019). Reverse osmosis desalination: a state-of-the-art review. *Desalination, 459*, 59–104. https://doi.org/10.1016/j.desal.2019.02.008

Ren, J., Sun, H., Cao, K., Ren, Z., Zhou, B., Wu, W., & Xing, F. (2021). Effects of natural seawater mixing on the properties of alkali-activated slag binders. *Construction and Building Materials, 294*, 123601. https://doi.org/10.1016/j.conbuildmat.2021.123601

Saillio, M., Baroghel-Bouny, V., & Barberon, F. (2014). Chloride binding in sound and carbonated cementitious materials with various types of binder. *Construction and Building Materials, 68*, 82–91. https://doi.org/10.1016/j.conbuildmat.2014.05.049

Shao, Y., Zhou, M., Wang, W., & Hou, H. (2013). Identification of chromate binding mechanisms in Friedel's salt. *Construction and Building Materials, 48*, 942–947. https://doi.org/10.1016/j.conbuildmat.2013.07.098

Shi, Z., Geiker, M. R., DeWeerdt, K., Østnor, T. A., Lothenbach, B., Winnefeld, F., & Skibsted, J. (2017). Role of calcium on chloride binding in hydrated Portland cement–metakaolin–limestone blends. *Cement and Concrete Research, 95*, 205–216. https://doi.org/10.1016/j.cemconres.2017.02.003

Shi, Z., Geiker, M. R., Lothenbach, B., De Weerdt, K., Garzon, S. F., Enemark-Rasmussen, K., & Skibsted, J. (2017). Friedel's salt profiles from thermogravimetric analysis and thermodynamic modelling of Portland cement-based mortars exposed to sodium chloride solution. *Cement and Concrete Composites, 78*, 73–83. https://doi.org/10.1016/j.cemconcomp.2017.01.002

Shi, Z., Shui, Z., Li, Q., & Geng, H. (2015). Combined effect of metakaolin and sea water on performance and microstructures of concrete. *Construction and Building Materials, 74*, 57–64. https://doi.org/10.1016/j.conbuildmat.2014.10.023

Shumuye, E. D., Zhao, J., & Wang, Z. (2019). Effect of fire exposure on physico-mechanical and microstructural properties of concrete containing high

volume slag cement. *Construction and Building Materials, 213*, 447–458. https://doi.org/10.1016/j.conbuildmat.2019.04.079
Son, H. M., Park, S. M., Jang, J. G., & Lee, H. K. (2018). Effect of nano-silica on hydration and conversion of calcium aluminate cement. *Construction and Building Materials, 169*, 819–825. https://doi.org/10.1016/j.conbuildmat.2018.03.011
Song, S., Zhang, N., Yuan, J., & Zhang, Y. (2021). New attempt to produce red mud-iron tailing based alkali-activated mortar: performance and microstructural characteristics. *Journal of Building Engineering, 43*, 103222. https://doi.org/10.1016/j.jobe.2021.103222
Suescum-Morales, D., Fernández, D. C., Fernández, J. M., & Jiménez, J. R. (2021). The combined effect of CO_2 and calcined hydrotalcite on one-coat limestone mortar properties. *Construction and Building Materials, 280*, 122532. https://doi.org/10.1016/j.conbuildmat.2021.122532
Sun, Y., Li, J., Chen, X., Huang, X., Guo, M., Wan, Y., Lu, L., Chen, Z., & Ma, Z. (2022). Preparation and characteristics of modified red mud-municipal solid waste incineration bottom ash binder. *Journal of Building Engineering, 46*, 103760. https://doi.org/10.1016/j.jobe.2021.103760
Torchette, B. (2007). Seagrass-salinity interactions: physiological mechanisms used by submersed marine angiosperms for a life at sea. *Journal of Experimental Marine Biology and Ecology, 350*, 194–215. https://doi.org/10.1016/j.jembe.2007.05.037
Trezza, M. A. (2007). Hydration study of ordinary Portland cement in the presence of zinc ions. *Materials Research, 10*(4), 331–334. https://doi.org/10.1016/j.cemconres.2009.01.017
Trezza, M. A., & Lavat, A. E. (2001). Analysis of the system $3CaO{\cdot}Al_2O_3$-$CaSO_4{\cdot}2H_2O$-$CaCO_3$-H_2O by FT-IR spectroscopy. *Cement and Concrete Research, 31*(6), 869–872. https://doi.org/10.1016/S0008-8846(01)00502-6
Ukrainczyk, N., Matusinovic, T., Kurajica, S., Zimmermann, B., & Sipusic, J. (2007). Dehydration of a layered double hydroxide—C2AH8. *Thermochimica Acta, 464*, 7–15. https://doi.org/10.1016/j.tca.2007.07.022
Villain, G., Thiery, M., & Platret, G. (2007). Measurement methods of carbonation profiles in concrete: thermogravimetry, chemical analysis and gammadensimetry. *Cement and Concrete Research, 37*(8), 1182–1192. https://doi.org/10.1016/j.cemconres.2007.04.015
Wang, J., Xie, J., Wang, Y., Liu, Y., & Ding, Y. (2020). Rheological properties, compressive strength, hydration products and microstructure of seawater-mixed cement pastes. *Cement and Concrete Composites, 114*, 103770. https://doi.org/10.1016/j.cemconcomp.2020.103770
Wang, Y., Shui, Z., Gao, X., Huang, Y., Yu, R., & Xiao, X. (2019). Modification on the chloride binding capacity of cementitious materials by aluminum compound addition. *Construction and Building Materials, 222*, 15–25. https://doi.org/10.1016/j.conbuildmat.2019.06.137
Wang, Y., Shui, Z., Gao, X., Yu, R., Huang, Y., & Cheng, S. (2019). Understanding the chloride binding and diffusion behaviors of marine concrete based on Portland limestone cement-alumina enriched pozzolans. *Construction and Building Materials, 198*, 207–217. https://doi.org/10.1016/j.conbuildmat.2018.11.270
Wang, Y., Ueda, T., Gong, F., & Zhang, D. (2019). Meso-scale mechanical deterioration of mortar due to sodium chloride attack. *Cement and Concrete Composites, 96*, 163–173. https://doi.org/10.1016/j.cemconcomp.2018.11.021
Yang, T., Fan, X., Gao, X., Gu, Q., Xu, S., & Shui, Z. (2022). Modification on the chloride binding capacity of alkali activated slag by applying calcium and aluminium containing phases. *Construction and Building Materials, 358*, 129427. https://doi.org/10.1016/j.conbuildmat.2022.129427
Yang, Y., Zhan, B., Wang, J., & Zhang, Y. (2020). Nondestructive assessment of the compressive strength of concrete with high volume slag. *Materials Characterization, 162*, 110223. https://doi.org/10.1016/j.matchar.2020.110223
Yang, Z., Gao, Y., Mu, S., Chang, H., Sun, W., & Jiang, J. (2019). Improving the chloride binding capacity of cement paste by adding nano-Al_2O_3. *Construction and Building Materials, 195*, 415–422. https://doi.org/10.1016/j.conbuildmat.2018.11.012
Yang, Z., Sui, S., Wang, L., Feng, T., Gao, Y., Mu, S., Tang, L., & Jiang, J. (2020). Improving the chloride binding capacity of cement paste by adding nano-Al_2O_3: the cases of blended cement pastes. *Construction and Building Materials, 232*, 117219. https://doi.org/10.1016/j.conbuildmat.2019.117219
Ylmén, R., & Jäglid, U. (2013). Carbonation of Portland cement studied by diffuse reflection fourier transform infrared spectroscopy. *International Journal of Concrete Structures and Materials, 7*(2), 119–125. https://doi.org/10.1007/s40069-013-0039-y
Ylmén, R., Jäglid, U., Steenari, B.-M., & Panas, I. (2009). Early hydration and setting of Portland cement monitored by IR, SEM and Vicat techniques. *Cement and Concrete Research, 39*(5), 433–439.
Yuan, Q., Shi, C., De Schutter, G., Audenaert, K., & Deng, D. (2009). Chloride binding of cement-based materials subjected to external chloride environment-a review. *Construction and Building Materials, 23*, 1–13. https://doi.org/10.1016/j.conbuildmat.2008.02.004
Zhang, J., Zhang, N., Li, C., & Zhang, Y. (2021). Strength development mechanism of a marine binding material with red mud and seawater. *Construction and Building Materials, 303*, 124428. https://doi.org/10.1016/j.conbuildmat.2021.124428
Zhang, T., Tian, W., Guo, Y., Bogush, A., Khayrulina, E., Wei, J., & Yu, Q. (2019). The volumetric stability, chloride binding capacity and stability of the Portland cement-GBFS pastes: an approach from the viewpoint of hydration products. *Construction and Building Materials, 205*, 357–367. https://doi.org/10.1016/j.conbuildmat.2019.02.026
Zheng, Y., Russell, M., Davis, G., McPolin, D., Yang, K., Basheer, P. A. M., & Nanukuttan, S. (2021). Influence of carbonation on the bound chloride concentration in different cementitious systems. *Construction and Building Materials, 302*, 124171. https://doi.org/10.1016/j.conbuildmat.2021.124171
Zhou, Y., Hou, D., Jiang, J., & Wang, P. (2016). Chloride ions transport and adsorption in the nano-pores of silicate calcium hydrate: experimental and molecular dynamics studies. *Construction and Building Materials, 126*, 991–1001. https://doi.org/10.1016/j.conbuildmat.2016.09.110
Zhu, Q., Jiang, L., Chen, Y., Xu, J., & Mo, L. (2012). Effect of chloride salt type on chloride binding behavior of concrete. *Construction and Building Materials, 37*, 512–517. https://doi.org/10.1016/j.conbuildmat.2012.07.079

Publisher's Note

Choonghyun Kang Choonghyu Kang is a Assistant Professor in Department of Ocean Civil Engineering at Gyeongsang National University. He is interested in the properties of construction materials, especially concrete materials. He is studying about crack propagation, tension-softening, crack analysis now.

Taewan Kim Taewan Kim is a Research Professor at the Department of Civil Engineering at Pusan National University. The major research areas are concrete structures and materials. Current interests are self-healing, ultra-lightweight concrete, eco-firendly cement and UHPC precast concrete construction technology.

Yong-Myung Park Yong-Myung Park is a Professor at the Department of Civil Engineering at Pusan National University. He mainly conducts research through experiments and FEM analysis on various concrete structures. He is particularly interested in reviewing and establishing design standards through FEM analysis of concrete and steel structures.

Ki-Young Seo Ki-Young Seo is in charge of research and development at HK E&C. He mainly works on the design, review, and automation of concrete structures, and also engages in patent registration through research and development on concrete. He is currently interested in developing eco-friendly concrete and modular concrete.